HOKKAIDO UNIVERSITY

Title	The influence of Si on the microstructure and sintering behavior of ultrafine WC
Author(s)	Kumar, A. K. Nanda; Watabe, Masaaki; Kurokawa, Kazuya
Citation	Philosophical Magazine, 92(32), 3950-3967 https://doi.org/10.1080/14786435.2012.700127
Issue Date	2012-07-10
Doc URL	https://hdl.handle.net/2115/52953
Rights	This is an Author's Accepted Manuscript of an article published in Philosophical Magazine, Volume 92, Issue 32, pages 3950-3967, 2012, © 2012 Taylor & Francis, available online at: http://www.tandfonline.com/10.1080/14786435.2012.700127
Type	journal article
File Information	PM92-32_3950-3967.pdf

Hokkaido University Collection of Scholarly and Academic Papers : HUSCAP

The influence of Si on the microstructure and sintering behavior of ultrafine WC

A K NANDA KUMAR[§]*, Masaaki WATABE[†] and Kazuya KUROKAWA[§]

[§] Laboratory of High Temperature Materials, Centre for Advanced Research of Energy and Materials, Hokkaido University, Sapporo, Japan – 060 8628.

[§]Ph.: +81-011-706-7572, Fax: +81-011-706-7119.

[†]Ohta Seiki Co. Ltd., Hokkaido, Japan 079-0314.

[†]Ph.: 0125-65-2759.

[§]*Corresponding author email id: aknk27@yahoo.com

[§]kurokawa@eng.hokudai.ac.jp

Abstract

The microstructure of sintered nano scale tungsten carbide powders with 1wt. % Si addition was found to be populated by an abnormally large number of elongated grains. Interrupted sintering experiments were conducted to clarify the origins of the excessive abnormal grain growth seen in the microstructure. It was observed that rapid coarsening occurred at high temperatures owing to the formation of a liquid phase. However, the grain shape evolution during this coarsening period was found to be a consequence of excessive stacking faults and micro twins on the basal planes probably generated by reaction of WC with Si. Analyses of the microstructures and the isothermal and non isothermal coarsening behaviors suggested that the platelet morphology evolved by defect-assisted nucleation and growth on faceted grains. Based on experimental evidence from samples interrupted at low temperatures and crystal growth theories, we discuss the possible mechanisms that eventually led to the rampant platelet-type morphology. Further, the influence of such rapid grain growth on the shrinkage rate during sintering is also discussed. In comparison with the cyclic coarsening-densification process of sintering in pure nano scale WC, the addition of Si leads to only two distinct sintering stages: either densification dominated or coarsening dominated. Concurrent densification and coarsening cannot be sustained particularly in the presence of a liquid phase that significantly enhances coarsening.

Keywords: nano WC-Si, abnormal grain growth, spark plasma sintering, faceting, platelets.

1. INTRODUCTION

Carbides of the transition metals of group IV-VI are generally characterized by high melting points and hardness and are therefore employed in applications wherein the thermo-mechanical stability of the component materials during operation is crucial. Often, certain ductile binder elements are added to the carbides leading to a duplex microstructure comprising a tough binder phase and a hard carbide phase (termed *cemented carbides*) which collectively improve the mechanical properties of the component. The microstructures of the carbide phase in such cemented carbides have often been found to be populated by angular, abnormal or coalesced grains [1-3]. Tungsten carbide (WC) with either Ni or Co binder is a candidate system of this class of cemented carbides and is one of the most industrially important abrasion and wear resistant carbides. Conforming to the general characteristics of the class of hexagonal cemented carbides, the microstructure of sintered WC-Co/Ni samples also evolves into abnormal and faceted grains during coarsening. Shape changes accompanying grain growth in the dual phase hexagonal carbides (WC-Co, WC-Ni and even pure WC) are usually attributed to the strong difference in surface energies between the prismatic and basal planes which subsequently lead to angular and faceted grains [4]. Secondary recrystallization or abnormal grain growth (AGG) is suspected to be a consequence of surface ledges produced by screw dislocations, stacking faults or twin defects on specific crystal planes which act as 2D nucleation sites for growth at later stages [5,6]. Coalescence in cemented WC seems to be an even more complex phenomenon arising as a result of faceting at early stages and AGG at later stages of sintering. Although theories of coalescence are not clearly established, experimental evidences and existing theories predict that in materials that tend to exhibit strong anisotropy in grain boundary

(GB) energies, coalescence may occur between contiguous grains with low GB misorientation angles [7,8].

Interestingly, GB faceting and AGG are observed even in pure and cemented nano grained WC (*n*-WC) although grain growth is restricted [9]. But generally, although faceting is common, the abnormally grown grains occupy only a small fraction of the total grains in cemented WC and are usually seen on the surface where the sample was in contact with the carbon die, suggesting that a change in the chemical activity (of C) can accompany or induce AGG [10]. Hence, certain pre-sinter processing methods have also been reported to avoid or reduce AGG [11].

In this paper, we report the influence of a small quantity (1 wt.%) of silicon binder on the microstructure of *n*-WC. The addition of Si was also found to suppress the formation of the brittle semi carbide phase (W_2C) during sintering as described in an earlier paper [12]. However, the microstructure after sintering was seen to be dominated by thin platelets as shown in **Figure 1a**. In comparison, the microstructure of sintered pure *n*-WC showed abnormal grains that were largely localized to the punch-sample interface (**Fig. 1b**) and only a few such abnormal grains were detected in the cross section of the samples. The addition of Si seems to lower the sintering temperature of pure *n*-WC, alter the chemical activity of the elements involved and consequently change the microstructure drastically. Understanding the mechanism of coarsening with the addition of Si to pure *n*-WC forms the chief motivation of this work. Moreover, such microstructures are interesting as AGG is reported to influence the mechanical properties of the compact [13]. Hence, to elucidate the origins of such platelet growth, the microstructural evolution was tracked by interrupting the sintering process at different temperatures. The results of the study are described in this paper.

2. EXPERIMENTAL DETAILS

Commercially purchased *n*-WC powders without any pre-treatment were used for sintering. The particle size measured by BET was 70 nm and the powder composition included 0.4% O, 5 ppm Cr, 27 ppm Fe, 4 ppm Mo, 3 ppm Ca, 2 ppm Ni, <5 ppm Si and < 2 ppm Sn. The *n*-WC powder was mixed with 1 wt. % Si powder (~5 μm average size and 99.9% purity) in a WC planetary ball milling unit for 30 minutes. Approximately 2.5 – 3 g of the powder was filled into a 10 mm diameter graphite die for spark plasma sintering (SPS) in a Dr SINTER LAB instrument. The SPS instrument has a dilatometer with an accuracy of 0.01 mm for measuring the instantaneous linear shrinkage. Temperature measurements were carried out using a radiation thermometer (pyrometer) that was focused on a small hole in the graphite die. Graphite sheets were used as spacers to separate the powder sample from the punch and die. After initial temperature stabilization at 873 K for 3 minutes, sintering was carried out in vacuum (< 4 Pa) at a constant heating rate of either 50 or 150 K/min and a compressive stress of 40 MPa. The sintering process was assumed to be complete when the dilatometer showed no further change in shrinkage during two successive temperature measurements. A set of samples were first obtained using a constant heating rate of 150 K/min and interrupting the sintering process at five different intermediate temperatures (1073 K, 1273 K, 1423 K, 1573 K and 1723 K) after which the samples were allowed to cool down to room temperature inside the vacuum chamber before being taken out. For isothermal coarsening studies, a non isothermal ramp to 1673 K at 50 K/min followed by isothermal hold for various time intervals ranging from 1–35 minutes was carried out. For the non isothermal coarsening studies, sintering was conducted at 50 K/min and interrupted at various high temperatures (1673 K, 1873 K and 2073 K). Before analysis,

the samples were first polished with fine diamond paste (1μm) and subsequently cleaned with ethanol in an ultrasonic bath. The densities of the samples were determined by the Archimedes method. All densities are reported relative to the density of pure WC (15.8 g/cc). Fractured (for low temperature microstructure evaluation) and etched samples (for coarsening studies) were used for the analysis. Before etching, the samples were cross sectioned, polished and cleaned as earlier. Conventional Murakami solution (H_2O+KOH+$K_3[Fe(CN)_6]$ in a volume ratio of 10:1:1) was used for etching the compacts. For TEM analysis, the cross sectioned samples were mechanically thinned to 100 μm, dimpled to a depth of 20 μm and then milled with Ar ions to electron transparency. Microstructure and phase analyses were carried out using XRD, EPMA, FE SEM and TEM. Grain size evaluation was performed using the FE SEM images (15000 X magnification) of the etched samples with the aid of an image analysis software (Image Pro-Plus). Approximately 150-200 grains from three different locations of a sample were randomly selected for the measurements. The boundaries were delineated either manually or auto segmented and the average diameter (average length of the diameters measured at 2° intervals and passing through the centroid of the selected grain) of the grains was calculated. The volume fractions of the abnormal grains were obtained by calculating the area fractions from the FE-SEM images (at 2500 X magnification). A minimum of three different images from each sample were analysed and the results presented in this paper are the average values thus obtained. The total area (volume) included the normal grains, abnormal grains and pores (i.e., % Normal grains + % Abnormal grains + % Pores = 100).

3. RESULTS

3.1 Sintering behavior

Figure 2 shows the shrinkage strain ($\Delta l/l_0$) and the measured relative density of the *n*-WC-Si sample interrupted at various temperatures. Initially there was a decrease in densification after which the shrinkage increased. The onset of densification occurred at around 1200-1300 K and the final sintering temperature (negligible change in rate of densification) was around 1723-1773 K, (as compared to the sintering temperature of 1873-2023 K in pure *n*-WC) depending on the heating rate and ambient pressure. Corresponding to the linear shrinkage, the measured density also showed an initial decrease followed by rapid densification. The initial decrease is attributed to thermal expansion and release of trapped gases within the green compact. **Figures 3a** and **3b** compare the shrinkage strains obtained in a few non isothermal experimental runs at different heating rates for both pure *n*-WC and *n*-WC with Si. Clearly, the addition of Si was found to induce rapid sintering in WC. The cross-over in the sintering trajectories occurred at around 1473 K, below which the shrinkage strains were almost similar in both samples. Very low heating rates (20 K/min and 10 K/min) were insufficient to induce significant densification in pure *n*-WC. Clearly, the end densification (sintering) temperatures were substantially lowered with the addition of Si (**Fig. 3c**). At low heating rates, the sintering temperatures of both *n*-WC and *n*-WC-Si were low and increased with the heating rate. However, with Si addition, the sintering temperature beyond 100 K/min was invariant at 1773 K. Using a temperature ramp rate of 10 K/min (not shown in **fig. 3c**), the exact sintering temperature with the addition of Si was found to be 1643 K. The final density of the *n*-WC-Si compact was 94% of the density of

pure WC (15.8 g/cc), while the pure *n*-WC powder could be sintered to nearly 100% density at the end of the sintering process.

3.2 Microstructure and phase analysis

Figure 4 shows the XRD of the samples interrupted at various stages of sintering. The initial powder contained a small fraction of the semi carbide (W_2C) phase which persists even at 1073 K. However, above 1073 K, the W_2C phase disappeared and low intensity peaks of tungsten oxide (WO_3) could be detected. From 1273 K to 1423K, along with the WO_3 phase, a tungsten silicon compound, W_5Si_3 was also detected in the sample. Above 1423 K, WO_3 disappeared completely, while the tungsten disilicide (WSi_2) phase was found to appear. Towards the end of sintering, there were no traces of WO_3 or W_2C and the final compact consisted of mainly WC and a low fraction of WSi_2. Interestingly, the other equilibrium phase SiC, was not detected in the X-ray diffraction analysis. However, EPMA composition mapping and line analysis near the Si inclusions revealed that in the sintered compact, Si had melted and the Si core was converted to SiC, establishing thermodynamic equilibrium (**Fig. 5a,b**). A large fraction of abnormal grains was also detected near the Si particles.

Sample microstructures of the compacts interrupted at various temperatures are shown in **figure 6(a-d)**. Grain growth was insignificant below 1573 K (although densification actively increased). After 1473 K, there was a sudden transition to well formed grain – pore structure (which corresponded with a decrease in the sintering strain). At 1723 K, few abnormal grains could be detected while at the end of the sintering stage (around 1773 K), there was massive abnormal grain growth aided by the molten Si phase. As observed in **Fig. 6d**, a large number of flat, plate-shaped grains

with well faceted edges can be clearly distinguished. Some of the large platelets also showed thin, straight delineating boundary lines. Packed between these large abnormally grown grains were the smaller grains with strong facets but low anisotropy. The pores were isolated and faceted and they also displayed unique geometries - triangular or rectangular - depending on whether they lie at the faceted grain boundaries or within the abnormal grains. Presence of pores within the abnormal grains suggests that the rate of coarsening far exceeds the rate of pore closure in this system.

Based on the experimental observations, the general microstructural evolution sequence can be summarized as follows:

T<1073 K: Oxidation of WC/W_2C and removal of CO_2;

1073K≤T≤1273 K: Formation of W_5Si_3 phase and oxidation of W to form WO_3;

1273K ≤T≤ 1423 K: Rapid increase in sintering rate, evaporation of WO_3, continuous formation of W_5Si_3 and nucleation of WSi_2 phase;

1423 K <T≤ 1573 K: Decrease in sintering rate, appearance of WSi_2, and grain growth of the WC microstructure into well formed pore-grain structure;

1623 K < T≤ 1773 K: Completion of sintering, sudden growth of platelet – type grains and well formed WC, stable W_5Si_3 and WSi_2 phases and conversion of Si particles to SiC.

Two facts are clear from the observations: (i) there is a strong tendency for Si to react with WC even at low temperatures and (ii) the platelet growth is supported only towards the end of sintering when the liquid phase forms. However, what demarcates this system is that unlike conventional liquid phase sintered samples of WC with Co/Ni binders, the degree of AGG is excessively high. The addition of Si seems to greatly enhance platelet formation and AGG leading us to suspect that the low temperature

reactions and the low formation energy of the W-Si compounds (ΔG_{W5Si3} = -360 kJ/mol) may have an influence on the rate of evolution and the nature of grain coarsening observed at high temperatures. A possible mechanism of chemical reaction assisted platelet growth is discussed in the following section within the framework of crystal growth theories.

4. DISCUSSION

4.1 Coarsening mechanism

Grain coarsening during high temperature sintering in the presence of a liquid phase is usually attributed to the Ostwald type solution-reprecipitation mechanism. The steady state time evolution of an initial particle size distribution (PSD) of average radius R_m is described by the classical LSW theory for both interface controlled and diffusion controlled coarsening [14]. The coarsening of normal angular grains of WC in the presence of liquid Co/Ni binders has been reported to be interface controlled [15]. Isothermal coarsening experiments at 1673 K revealed that the PSD in the *n*-WC-Si samples indeed followed a log-normal distribution independent of the holding time and irrespective of whether the grains sampled were platelets or small grains (**Fig. 7**). The only difference was the order of magnitude change in the average grain size of the PSDs which underwent a drastic change as platelets grew at temperatures near the melting point of Si. Within a minute of isothermal hold at 1673 K, the platelets grew to ~3.5 μm length and saturated thereafter. The volume fraction of the abnormal grains also followed a similar behavior as shown in **Fig. 8a**, reaching saturation at ~30%. After sudden nucleation of the abnormal grains at the very beginning of the isothermal hold period, the interlocking microstructure that develops subsequently prevents further

growth of the abnormal grains and hence the coarsening kinetics becomes almost stagnant. On the other hand, the non isothermal coarsening experiments revealed a continuous increase in the dimensions of the platelets but a saturation of the volume fraction of the abnormal grains to nearly 50% at 2073 K (**Fig. 8b)**. The dimensions of the abnormal grains increase progressively with temperature (and hence the W-Si liquid phase fraction) while the fraction of abnormal grains tends to saturate under both isothermal and non-isothermal sintering conditions. This behavioral trend is consistent with that observed by Rios et al [16] and Afshar and Simchi [17] for abnormal grains at elevated temperatures in the $BaTiO_3$-TiO_2 and Al_2O_3-Cu systems, respectively. However, while the AGG mechanism in both their cases was argued to be GB pinning (the abnormal grains were also isotropic), we rule out this mechanism in the *n*-WC-Si system as discussed below.

The classical LSW theory does not account for such AGG since it predicts that grains with a radius, $R>2R_m$ will have a zero growth rate and hence runaway growth is not possible. Theories of AGG (for example [18]) suggest that such phenomena can occur when (i) normal grain growth is inhibited by the presence of second phase particles (GB pinning) or (ii) there is at least one grain that is much larger than the others (seeding) or (iii) the nucleation/growth mechanism is vastly different in a particular subset of grains when compared to the rest of the grains (2D nucleation).

In the present case, the investigated platelets were indeed found to be surrounded by one or two faceted WSi_2 crystals (**Fig. 9**). These secondary phases conveniently form on the slowly growing W-rich basal planes of the WC unit cell with an orientation relation of the type $\{002\}_{WSi2}$ // $\{\bar{1}2\bar{1}0\}_{WC}$. However, for AGG by GB pinning, a more uniform coverage by second phase particles is expected. Moreover,

while the W-Si phases are detected even at low temperatures (T>1073 K), AGG is observed only at higher temperatures (~1673 K) when the liquid phase is expected to form (the lowest eutectic temperature in the W-Si binary system is 1663 K). Likewise, the AGG mechanism is of a rapid, burst-type character which is quite distinct from what one would expect had the mechanism been controlled solely by GB pinning. Therefore, the formation of W-Si compounds near the platelets suggests a strong alteration of the chemical nature of W in the platelets rather than runaway growth by GB pinning. No clear evidence of agglomerates or large grains was observed at temperatures just below the abnormal grain - forming temperature, confirming that the AGG mechanism by seeding also could not have occurred. The presence of a thin fault line between the platelets and the anisotropic nature of the abnormal growth readily points to a mechanism of AGG by defect-assisted 2D nucleation.

According to the previous discussion, platelet growth in *n*-WC-Si can evolve under two conditions: flat interfaces and large defect densities. A faceted, 'candidate' crystal of WC is generally bounded by the {0001} basal and $\{10\bar{1}0\}$ prism planes. Under normal conditions, the degree of super saturation in the surrounding liquid phase has to be excessively high for the 2D nucleation mechanism to be operative. Crystal growth theories predict that the growth rate of a facet by pure 2D nucleation is proportional to $\exp(-\pi\varepsilon^2/k_B T h\Delta G)$, where ε ($\approx h\gamma_{s\text{-}l}$) is the edge energy of a disc shaped nucleus, $\Delta G = 2\Omega\gamma_{s\text{-}l}\,(1/R_a - 1/R)$ is the driving force for coarsening of a grain of radius R in a matrix of grains with critical radius R_a, h is the height of the nucleus, $\gamma_{s\text{-}l}$ is the solid-liquid interface energy, Ω is the atomic volume and the rest of the terms have the usual meanings. However, the presence of a surface defect can greatly reduce the critical driving force required for 2D nucleation. For instance, the growth rate, v, of a

crystal facet assisted by a screw dislocation is given by v=A. ($\Delta G^2/\varepsilon$). tanh ($\varepsilon/\Delta G$) [19]. Similarly, it has been suggested that for a 2D nucleus formed on a re-entrant edge, the edge energy is altered by a factor of $(\theta - \sin\theta\cdot\cos\theta)/\pi$, where θ is the angle subtended by the growing nucleus on the re-entrant edge [20].

Figure 10 shows the hypothetical growth rates for a model system of grains that have singular (2D nucleation) and varying degrees of vicinal (defect assisted) interfaces. As can be seen, the growth rate increases exponentially after a critical radius is crossed. In the presence of a crystallographic defect such as a screw dislocation or a re-entrant edge, the critical radius necessary for AGG is reduced, readily leading to anisotropic runaway grain growth by 2D nucleation.

The platelet growth in *n*-WC-Si was found to be defect-assisted (defect by twinning). Observation of the final sintered samples indicated that the platelets are always bounded by the basal (0001) and prismatic ($10\bar{1}0$) planes (**Fig. 11**). They comprise a pair of thin crystals with a common (0001) plane. To investigate the stage where defects evolved, a sample sintered at 1323 K for 30 minutes was observed with a TEM. The observation showed a high density of slip bands enclosing stacking faults (SFs) between split partials in the microstructure. Although grain growth was limited and faceting was not discernible, almost the entire microstructure consisted of grains with a high density of planar defects lying mostly on the prismatic planes which is the general twinning plane in hcp carbides (**Fig. 12a**). This low temperature microstructure was common irrespective of the addition of Si; for instance, **Fig. 12b** shows the microstructure of a pure *n*-WC sample sintered at 1323 K for 30 minutes showing similar stacking faults and twins on the prismatic planes. Hence it is quite apparent that at low temperatures the microstructure of *n*-WC-Si is not largely different from that of

pure *n*-WC. This naturally suggests that the effect of silicon is significant only at higher temperatures and that the defect structure on the basal planes is brought about by the addition of Si. Although ball milling of the powder (with Si) could have led to a slight increase in the density of SFs in the microstructure, it does not explain the fact that the thin SFs and twins were observed on the basal planes in the final sintered compact (as shown earlier in **Fig. 11**) rather than on the prism planes as observed in the low temperature sintered samples shown in **Fig. 12a**. This leads us to strongly suspect that there could be other mechanisms responsible for generating SFs at high temperatures other than those purely driven by stress.

A possible defect generation mechanism for the high temperature SFs on the basal planes can be assumed to originate as follows (schematic shown in **Fig. 13)**: in the reaction between WC and Si, the formation of W-Si compounds is favored due to their low formation energies. This is supported by the experimental observation that the W_5Si_3 compound can be detected even at 1323 K when the sintering process is still in the solid state and that their volume fraction increases continuously with increasing temperature. However, the formation of such compounds leads to a plane of W-vacancies in the WC unit cell. Vacancies in hcp structures usually tend to precipitate on the close packed (0001) basal planes. To compensate the deviation in stoichiometry, the excess C has to be eliminated by reacting with oxygen from the atmosphere, and forming volatile CO/CO_2 gases. However, if such a compensation reaction was inhibited (possible under conditions of low pressure as in the present experiments or due to the strong bonding between W-C atoms (7.9 eV) [21]), the excess C can still remain in the unit cell forming a C-terminated plane. This results in two similar layers coming into contact leading to a high energy configuration and is avoided by either altering the

stacking sequence above and below the vacancy plane or by introducing a partial dislocation loop so that the arrangement is energetically stable. This is equivalent to a displacement of 1/3<0$\bar{1}$10>, which moves the C atoms to the next symmetric position in the unit cell. The SF accommodation seems to be favored in the *n*-WC-Si system since the presence of such a single or double faulted structure leads to a twinned-lattice relation at further stages of growth [22]. Such types of SF assisted twinned grains can easily introduce re-entrant edges on the surface of the growing grain, which assists AGG when the liquid phase is formed. However, the presence of Si could not be detected at the platelet junction and it is not known whether the platelet configuration is stabilized into a lower energy state by the formation of a monolayer of Si-C between the platelets, which has an almost equal free energy of formation at T>1673 K ($\Delta G\,|_{WC/SiC}$ = -45 kJ/mol) .

Irrespective of the generation mechanism, the SF or twin defect terminating at the grain surface provides a re-entrant edge on the (10$\bar{1}$0) planes to assist 2D nucleation. In the presence of a liquid phase, coarsening is accelerated leading to sudden AGG and a massive transformation of the microstructure to a platelet-type morphology. Moreover, liquid Si does not wet WC grains uniformly. The wetting angle of liquid Si on WC has been reported to be 30° implying that some crystal facets might be more favorable for liquid Si to penetrate than others [23]. Under such anisotropic wetting conditions, supersaturation occurs only on certain planes thereby increasing the probability of nucleation and growth along specific directions leading to a highly anisotropic microstructure.

At higher temperatures (T>1673 K), a second mechanism of coalescence-induced grain coarsening was also observed to be active whereby faceted grains stack together and quickly reduce their grain boundary areas. Under favorable conditions, this mechanism leads to rapid grain growth by coalescence and formation of the unique pore geometries observed in the samples (**Fig. 14a**). The particle rearrangement mechanism also leads to clustering of faceted grains with unfavorable orientations (**Fig. 14b**). Both the clustering and coalescence type of microstructures are observed only after the Si melt is formed reaffirming the strong effect of the liquid phase in reducing intergranular friction. This leads to grain sliding and rotation so that contiguous faceted grains realign to form clusters with low or high misorientation angles. The clusters seem to form by a type of particle rearrangement process preferentially along the prismatic planes ($\{10\bar{1}0\}$) rather than the basal planes. Coalescence along $\{0001\}$-$\{10\bar{1}0\}$ are also observed in some clusters as the c/a ratio of WC is close to unity. The faceted pores formed by AGG and by coalescence mechanisms are generally difficult to sinter due to their flat surfaces and small pore co-ordination numbers and thereby contribute to the low final densities.

4.2 Effect of coarsening on the sintering behaviour

The influence of sudden AGG and coarsening on the sintering behavior is clearly evident when the grain size evolution is compared with the sintering rate at various temperatures. Owing to the strong anisotropy in the microstructure of *n*-WC-Si, the average length and width of the plate-like grains are shown along with the aspect ratio (**Fig. 15a**). Significant grain growth occurs above 1573 K. But the rapid grain growth results in a simultaneous decrease in densification rate. Although grain growth and densification are governed by different driving forces, the transition nature of these

curves indicates that both processes occur simultaneously at high temperatures. Pores trapped within abnormal grains and faceted pores within clusters are difficult to sinter, and they consequently reduce the densification rate. In a previous work, we had shown that in the case of pure *n*-WC, a small amount of coarsening is necessary for densification to progress in the intermediate stage due to the formation of agglomerates [24]. Slow coarsening combined with agglomeration leads to a cyclic densification-grain growth mechanism which eventually results in a multi-staged sintering process evidenced by transient regions of varying slopes in the shrinkage rate – temperature graph. However, in the presence of Si, irrespective of agglomeration, rapid coarsening sets in so that only two distinct stages occur: an initial stage where densification is the dominant mechanism and a second stage where densification drops drastically as grain growth increases (**Fig. 15b**). The fast coarsening rate in the presence of Si may be responsible for the abrupt decrease in densification rate.

5. CONCLUSION

The sintering behavior of *n*-WC-Si has been analyzed by interrupting the sintering process. Presence of Si enhances AGG, leading to an almost explosive growth of platelets at temperatures near to its melting point. The coarsening behavior can be satisfactorily explained on the basis of theories of crystal growth aided by a liquid phase. While sintered WC compacts (with or without Co/Ni binders) generally show a strong tendency for faceted growth and little AGG, the extensive platelet growth observed with a small addition of Si marks a unique behavior of WC whose origins can probably be traced back to a combination of both chemical and microstructural factors. The densification behavior of *n*-WC-Si is also different when compared with that of pure *n*-

WC. Rapid coarsening aided by a liquid phase at high temperatures along with the formation of faceted pores strongly retards densification beyond 1573 K. The interlocking microstructure observed in the final sintered sample can also be expected to influence the mechanical properties of the sample by altering its fracture toughness. Such features may be worth investigating in further detail owing to the necessity of a tougher and harder WC compact for applications in industries.

References

[1] G. Grathwohl and R. Warren, Mater. Sci. Eng. A 14 (1974) p. 55.

[2] H.M. Wang, L.G. Yu, X.X. Li and P. Jiang, Sci. Tech. Adv. Mater. 2 (2001) p. 173.

[3] Y. Chen and H.M. Wang, Mater. Lett. 57 (2003) p. 1233.

[4] A.V. Shatov, S.A. Firstov and I.V. Shatova, Mater. Sci. Eng. A 242 (1998) p. 7.

[5] T. Li, Q. Li, L. Lu, J.Y.H. Fuh and P.C. Yu, Phil. Mag. A 87 (2007) p. 5657.

[6] B.K. Yoon, Bo-Ah Lee and Suk-Joong L. Kang, Acta Mater. 53 (2005) p. 4677.

[7] W.A. Kaysser, S. Takajo and G. Petzow, Acta Metall. 32 (1984) p. 115.

[8] S. Takajo, W.A. Kaysser and G. Petzow, Acta Metall. 32 (1984) p. 107.

[9] Z. Zak Fang, X. Wang, Taegong Ryu, Kyu Sup Hwang and H.Y. Sohn, Int. J. Refract. Met. Hard Mater. 27 (2009) p. 288.

[10] L. Girardini, M. Zadra, F. Casari and A. Molinari, Met. Pwdr. Rep. 63 (2008) p. 18.

[11] Dong-Yeol Yang and Suk-Joong L. Kang, Int. J. Refract. Met. Hard Mater. 27 (2009) p. 90.

[12] A.K. Nanda Kumar, M. Watabe, A. Yamauchi, A. Kobayashi and K. Kurokawa, Trans. JWRI 39 (2010) p. 47.

[13] Tao Li, Q. Li, J.Y.H. Fuh, P.C. Yu, L. Lu and C.C. Wu, Mater. Sci. Eng. A 445-446 (2007) p. 587.

[14] M.N. Rahman, *Ceramic Processing and Sintering*, 2nd ed., Marcel Dekker Inc., New York, 2003.

[15] X. Wang, Z. Fang and H.Y. Sohn, Int. J. Refract. Met. Hard Mater. 26 (2008) p. 232.

[16] P.R. Rios, T. Yamamoto, T. Kondo and T. Sakuma, Acta Mater. 46 (1998) p. 1617.

[17] Amir Afshar and A. Simchi, Scripta Mater. 58 (2008) p. 966.

[18] M. Hillert, Acta Metall. 13 (1966) p. 227.

[19] J.P. Hirth and G.M. Pound, *Condenstation and evaporation: Nucleation and growth kinetics*, in *Progress in Materials Science II*, Bruce Chalmers, eds., Pergamon Press, Oxford, 1963, p.86.

[20] Kyung-Sik Oh, Jae-Yong Jun and Doh-Yeoh Kim, J. Am. Ceram. Soc. 83 (2000) p. 3117.

[21] Jiuxing Zhang, G. Zhang, S. Zhao and X. Song, J. Alloy. Compd. 479 (2009) p. 427.

[22] Michael Sommer, Wolf-Dieter Schubert, Erich Zobetz and Peter Warbichler, Int. J. Refract. Met. Hard Mater. 20 (2002) p. 41.

[23] G.A.Yasinskaya, Translated from *Poroshkovaya Metallurgiya*, 7-43 (1986) p. 53.

[24] A.K. Nanda Kumar, M. Watabe and K. Kurokawa, Ceram. Int. 37 (2011) p. 2643.

List of Figures:

Fig. 1. Microstructures of sintered compacts of (a) *n*-WC-Si and (b) *n*-WC.

Fig. 2. Relative densities and linear shrinkage strain of the sintered samples.

Fig. 3. Non isothermal linear shrinkage strain of *n*-WC and *n*-WC-Si at (a) 20 K/min and (b) 50 K/min and (c) Comparison of sintering temperatures of pure *n*-WC and *n*-WC-Si.

Fig. 4. XRD pattern of *n*-WC-Si compacts interrupted at various sintering temperatures. Strong unmarked peaks are from WC phase.

Fig. 5a. EPMA composition map of *n*-WC-Si near a Si particle after sintering and etching.

Fig. 5b. Line analysis of *n*-WC-Si sintered compact

Fig. 6. Representative microstructures of *n*-WC-Si compacts interrupted at various temperatures.

Fig. 7. Evolution of PSD with time for a sample sintered at 1723 K (numbers on the curves represent minutes of isothermal hold)

Fig. 8. (a) Growth kinetics of length and width and volume fraction of abnormal grains (1673 K) and **(b)** change in dimensions and volume fraction of abnormal grains at different temperatures for 0 min hold time. The SEM image in (b) is a sample microstructure sintered at 2073 K showing perfectly faceted grains along with abnormal grains. The distance marker represents 10 μm.

Fig. 9. Formation of WSi_2 on the basal (0001) planes of the WC platelets: **(a)** and **(b)** show two such platelets that were investigated which clearly accommodate W-Si compounds on their basal planes; **(c)** is the centred DF image of the WSi_2 grain in (b) and **(d)** is the corresponding SAD pattern with zone axis along <002> of WSi_2.

Fig. 10. Dependence of critical grain size for AGG calculated for flat and various vicinal crystal surfaces (an arbitrary value of r_0=0.5 μm was taken as the initial grain size for the calculation).

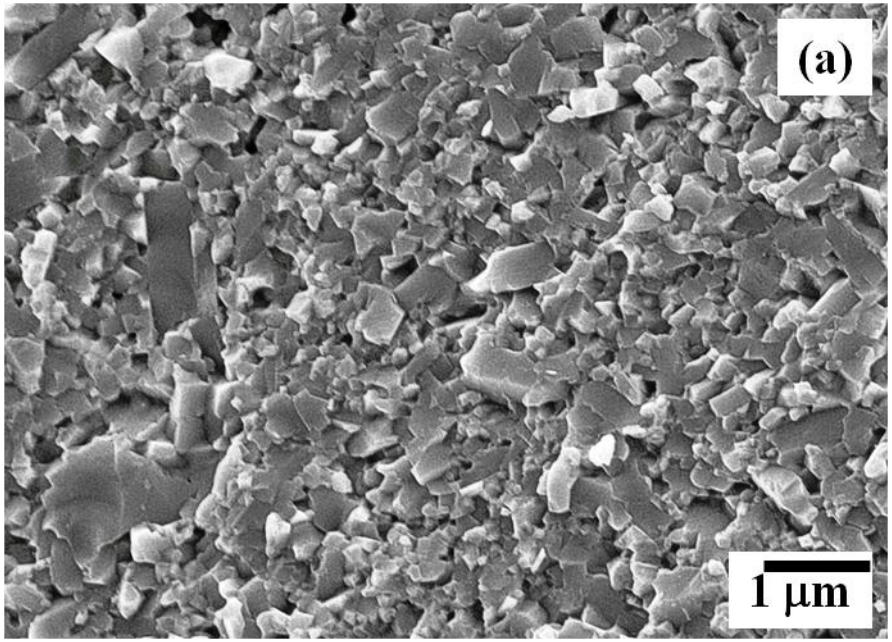
Fig. 11. TEM image of a cluster of large anisotropic grains surrounded by smaller faceted grains. (Right) DF image and corresponding SAD of a platelet pair.

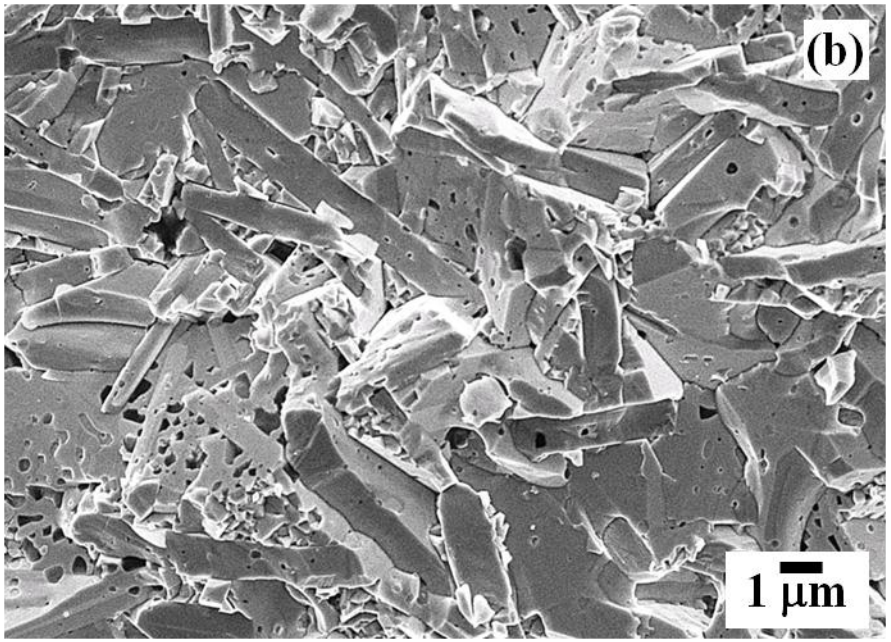
Fig. 12. (a) Microstructure of *n*-WC-Si sintered for 30 minutes at 1323 K; **(b)** *n*-WC sintered at 1323 K for 30 minutes. Both samples show extensive SFs on the prismatic planes as can be gleaned from the SAD patterns of pure *n*-WC-Si in **(c)** and *n*-WC in **(d)**. The patterns were imaged along the basal [0001] zone axis and profuse streaking is observed along the prism plane <10$\bar{1}$0> vectors (arrowed).

Fig. 13. Intrinsic atomic arrangement in WC-Si that evolves into platelets connected by a double twin: atomic configurations when projected along the [$\bar{1}$2$\bar{1}$0] direction. Red - W and Blue - C atoms. The dull colors represent missing atoms. An odd number of stacking faults leads to a single twin while even leads to a double twin. The final image is an actual TEM micrograph of a platelet pair.

Fig. 14. (a) Coalescence of grains (indicated by arrows) in a WC-Si sample sintered at 1823 K and **(b)** clustering of facetted grains in the same sample.

Fig. 15. (a) Variation of grain growth and shrinkage rate with temperature and **(b)** Linear densification strain rate of pure *n*-WC compared with *n*-WC-Si.





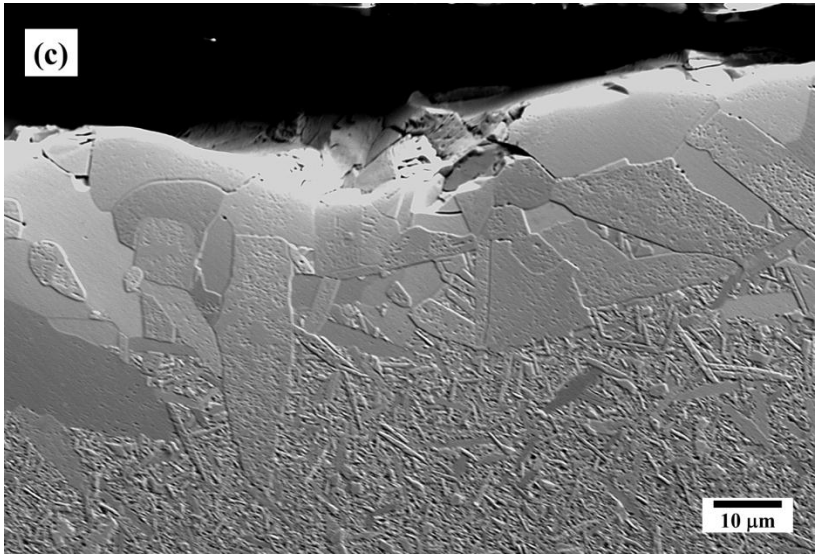


Fig. 1

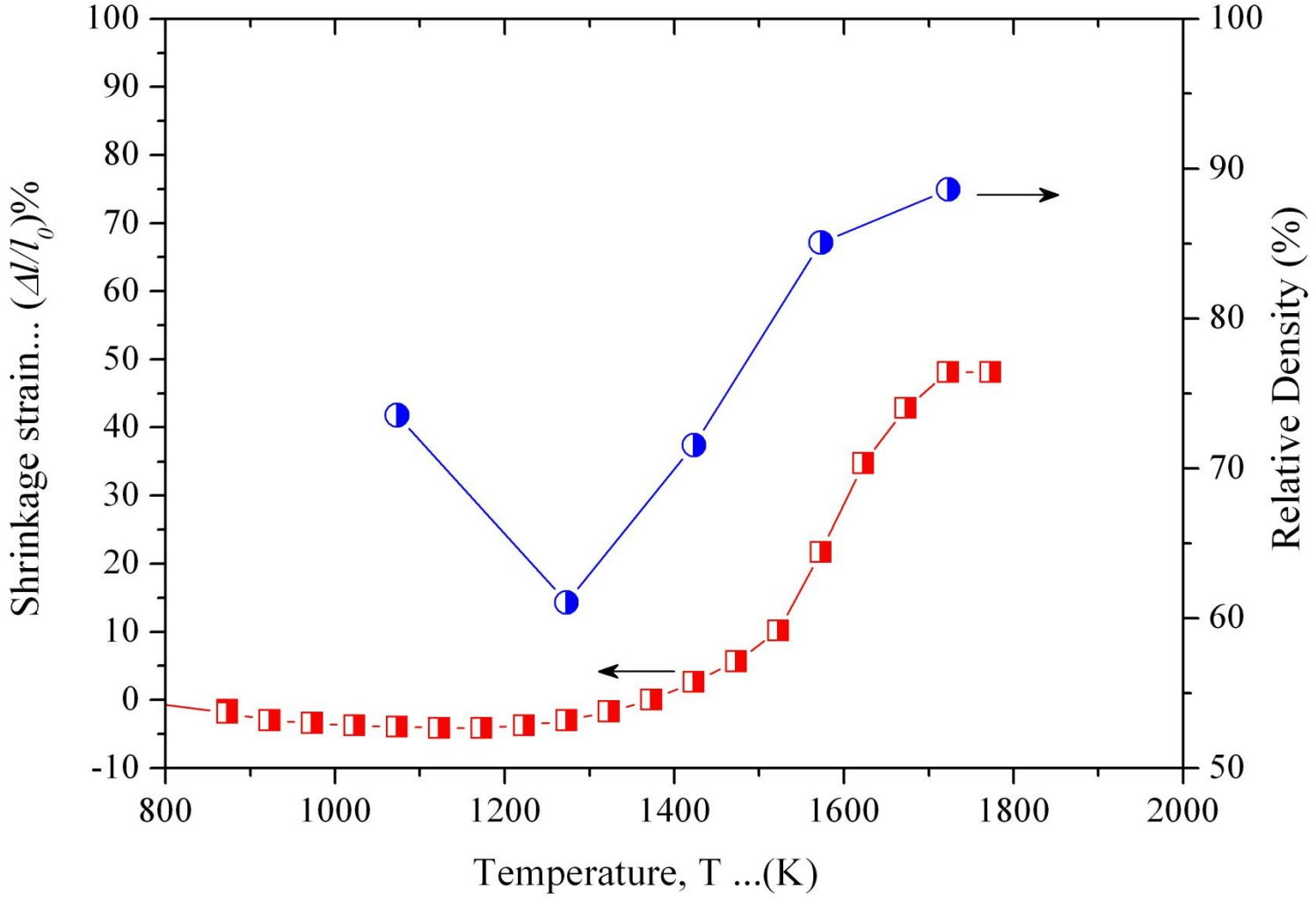

Shrinkage strain... ($\Delta l/l_0$)%
Relative Density (%)
Temperature, T ...(K)
100
90
80
70
60
50
40
30
20
10
0
-10
800
1000
1200
1400
1600
1800
2000

Fig. 2

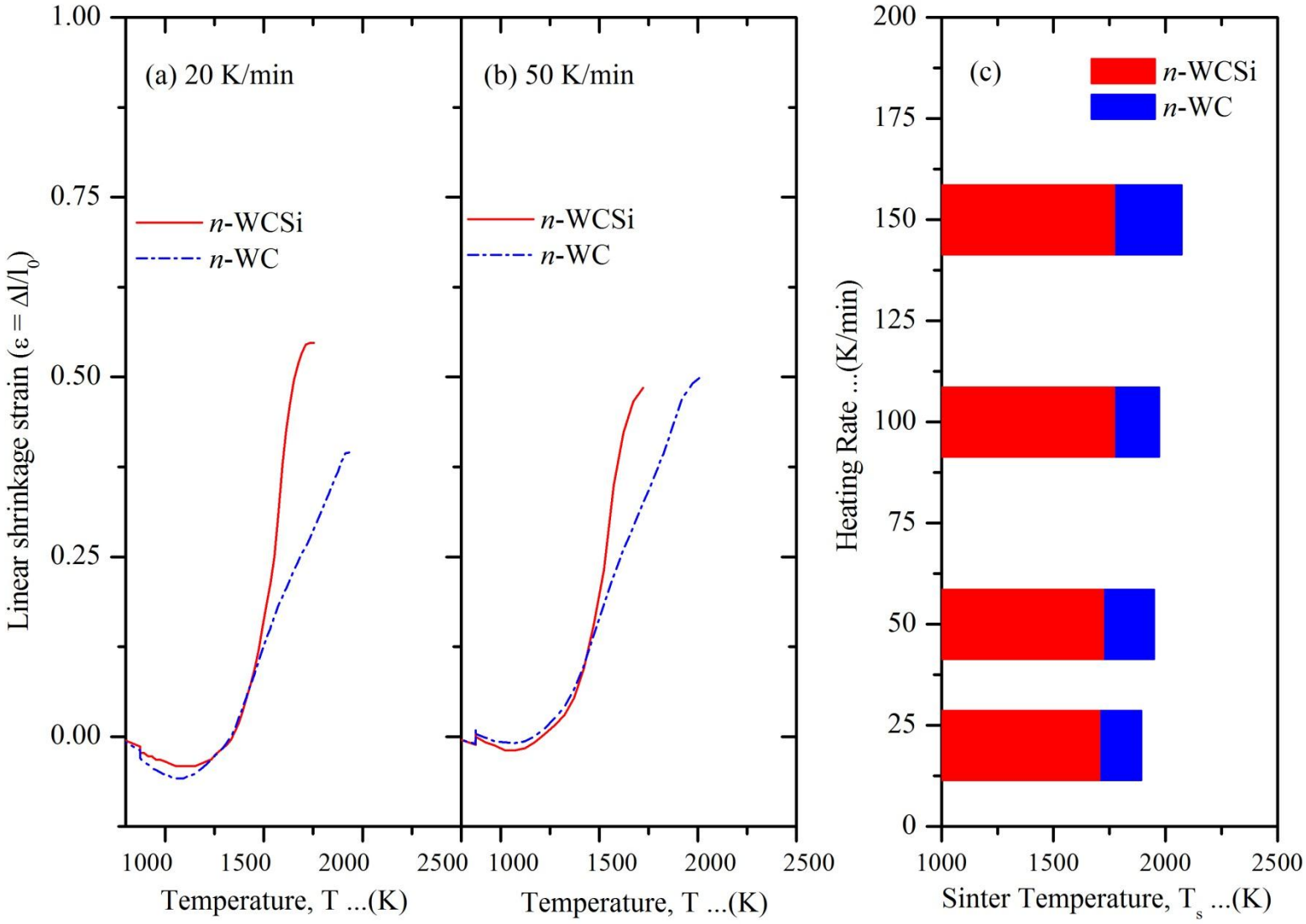

(a) 20 K/min
(b) 50 K/min
(c)
n-WCSi
n-WC
Linear shrinkage strain (ε = Δl/l0)
Heating Rate ...(K/min)
Temperature, T ...(K)
Sinter Temperature, Ts ...(K)
1.00
0.75
0.50
0.25
0.00
200
175
150
125
100
75
50
25
0
1000
1500
2000
2500

Fig. 3

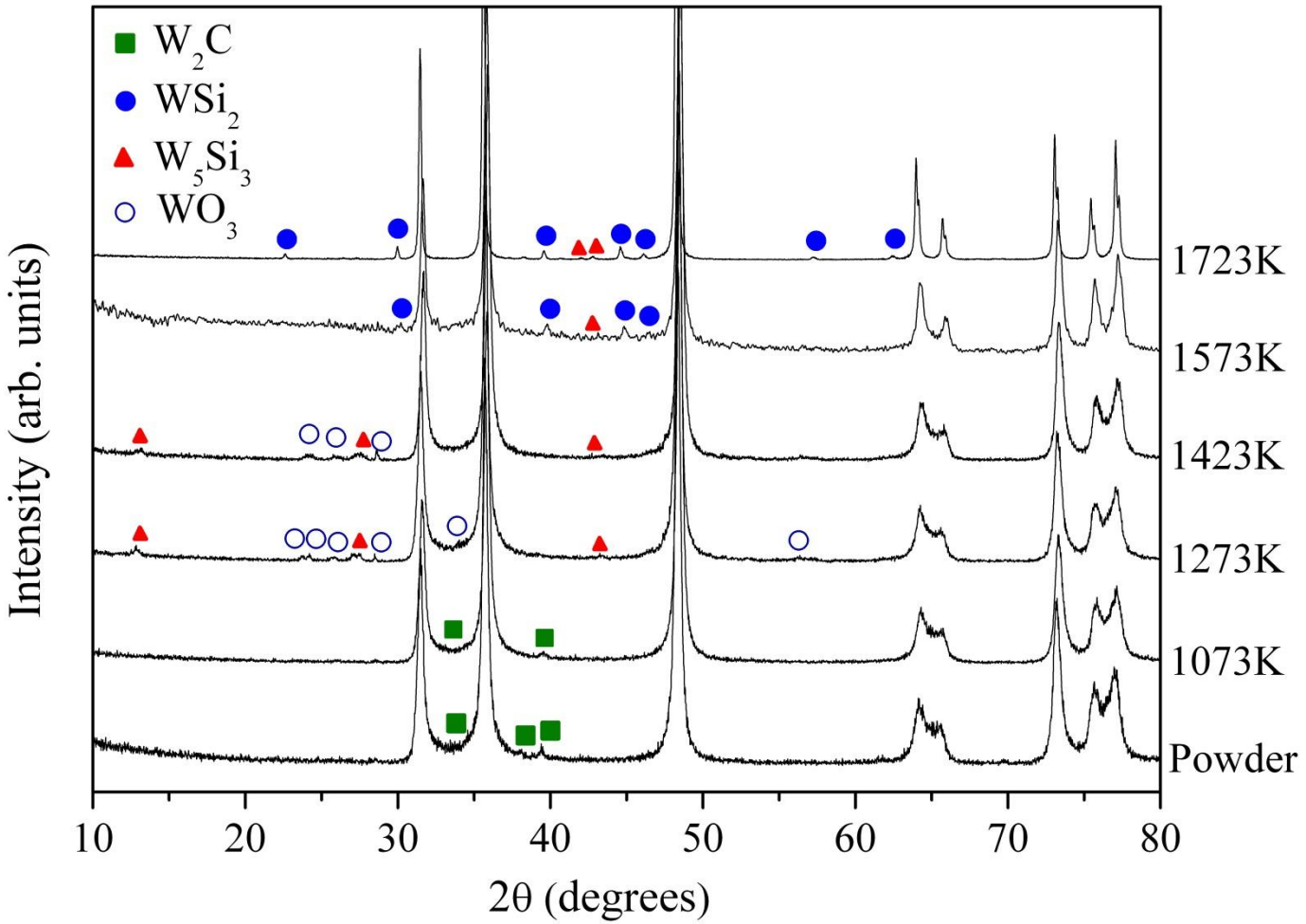
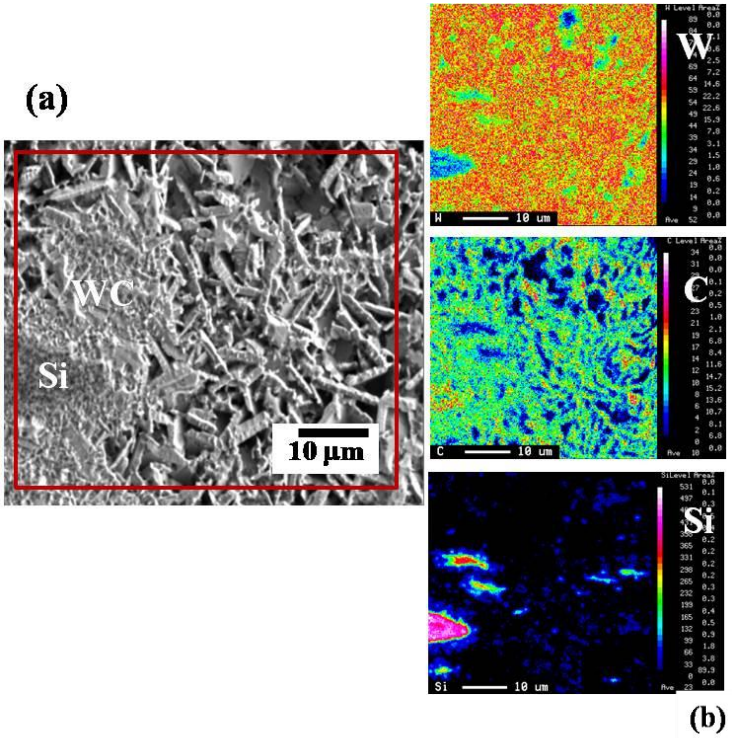
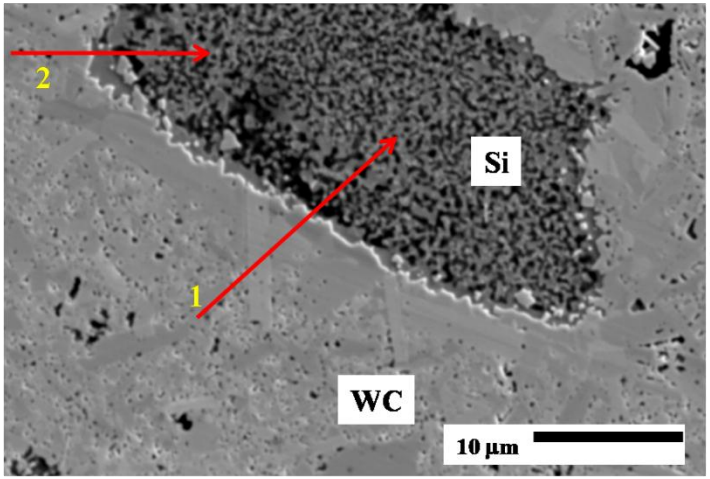
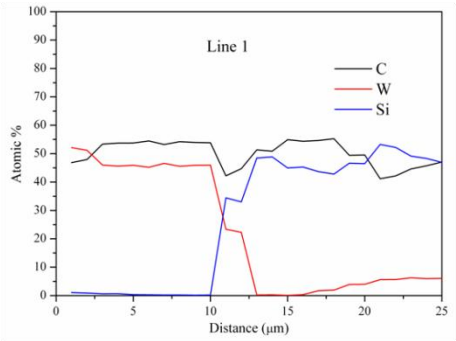

W2C
WSi2
W5Si3
WO3
1723K
1573K
1423K
1273K
1073K
Powder
Intensity (arb. units)
10
20
30
40
50
60
70
80
2θ (degrees)

Fig. 4


(a)
WC
Si
10 µm
W
10 µm
C
10 µm
Si
10 µm
(b)


2
1
Si
WC
10 µm


Line 1
C
W
Si
Atomic %
Distance (µm)

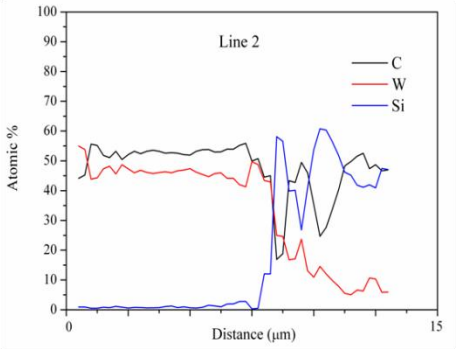

Line 2
C
W
Si
Atomic %
Distance (µm)

Fig. 5

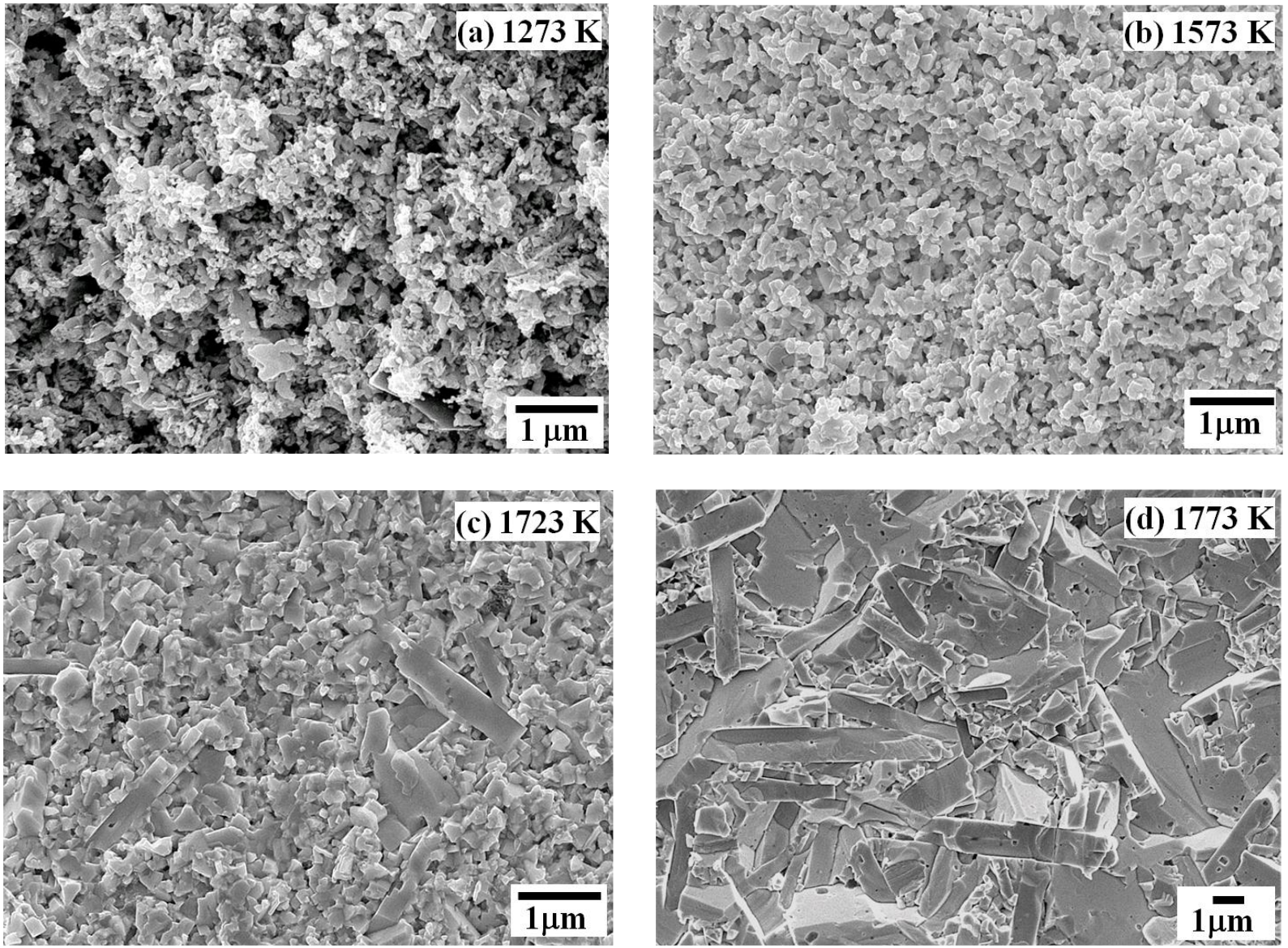


Fig. 6

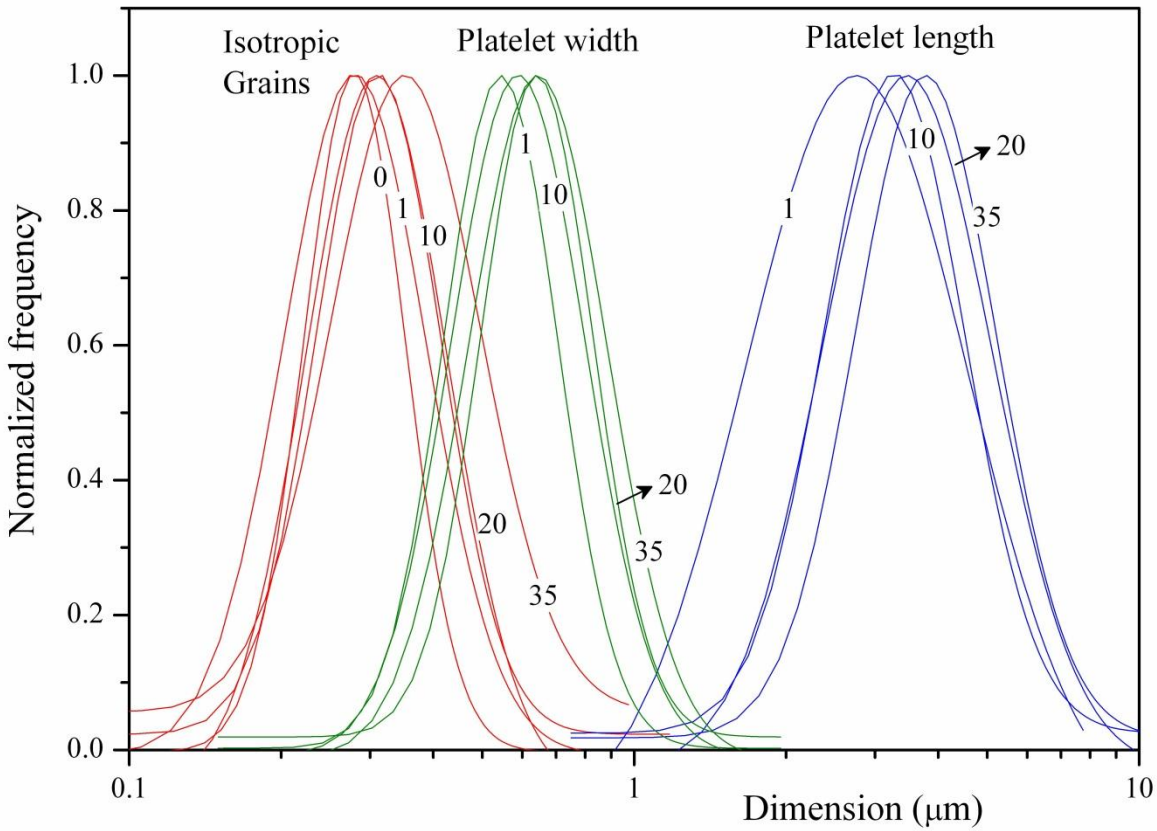

Isotropic
Grains
Platelet width
Platelet length
Normalized frequency
Dimension (μm)
1.0
0.8
0.6
0.4
0.2
0.0
0.1
1
10
0
1
10
20
35
1
10
20
35
1
10
20
35

Fig. 7

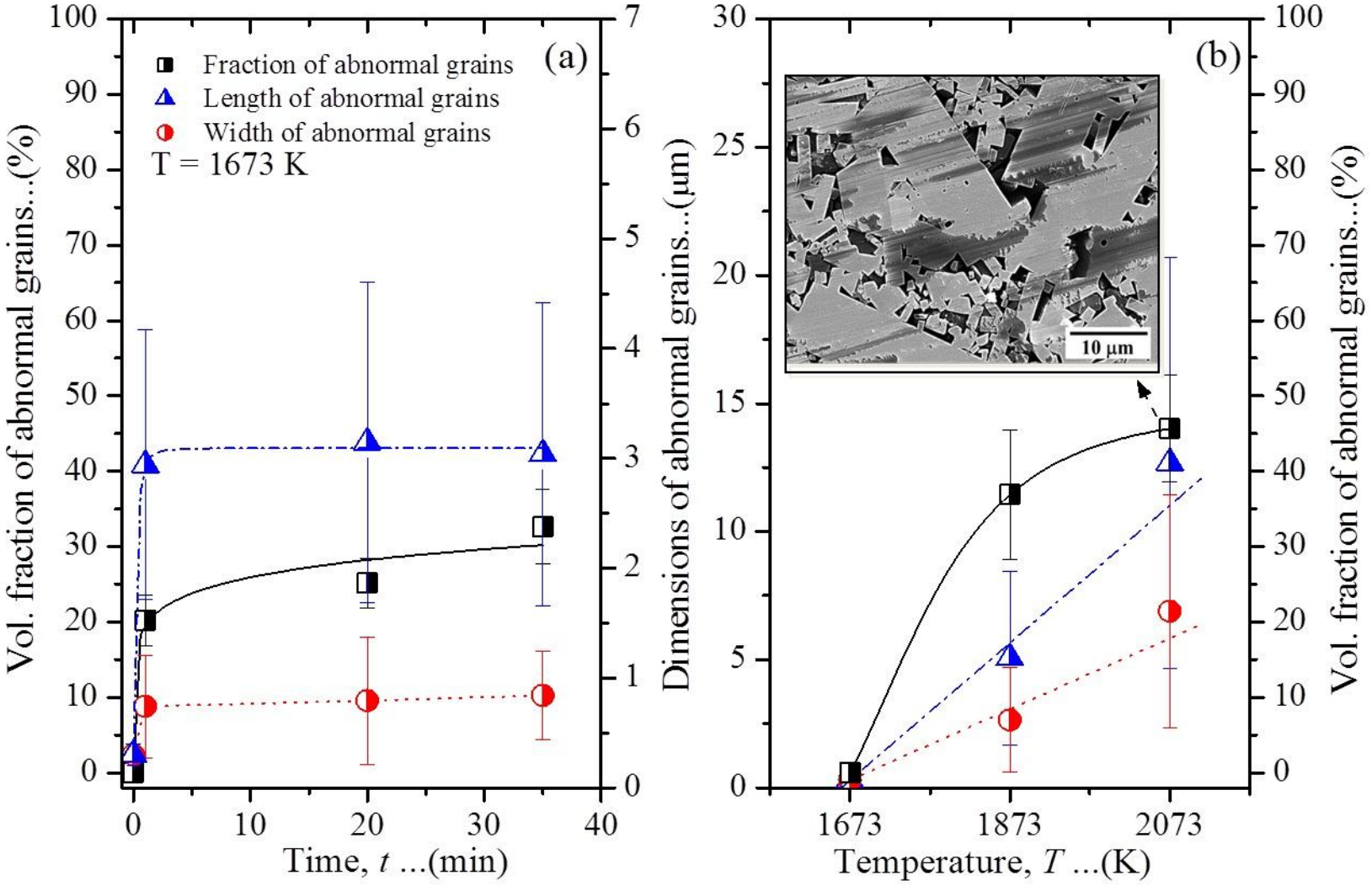

(a)
Fraction of abnormal grains
Length of abnormal grains
Width of abnormal grains
T = 1673 K
Vol. fraction of abnormal grains...(%)
Time, t ...(min)
(b)
10 μm
Dimensions of abnormal grains...(μm)
Vol. fraction of abnormal grains...(%)
Temperature, T ...(K)

Fig. 8

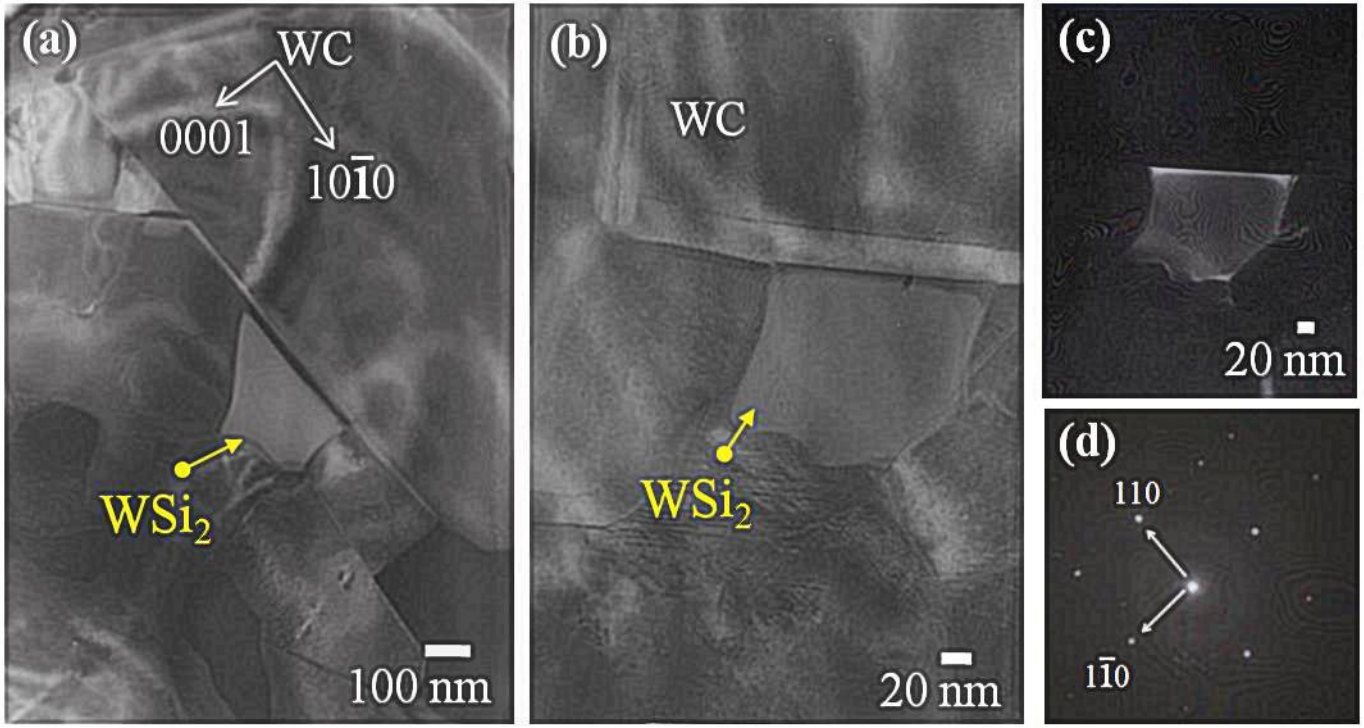


Fig. 9

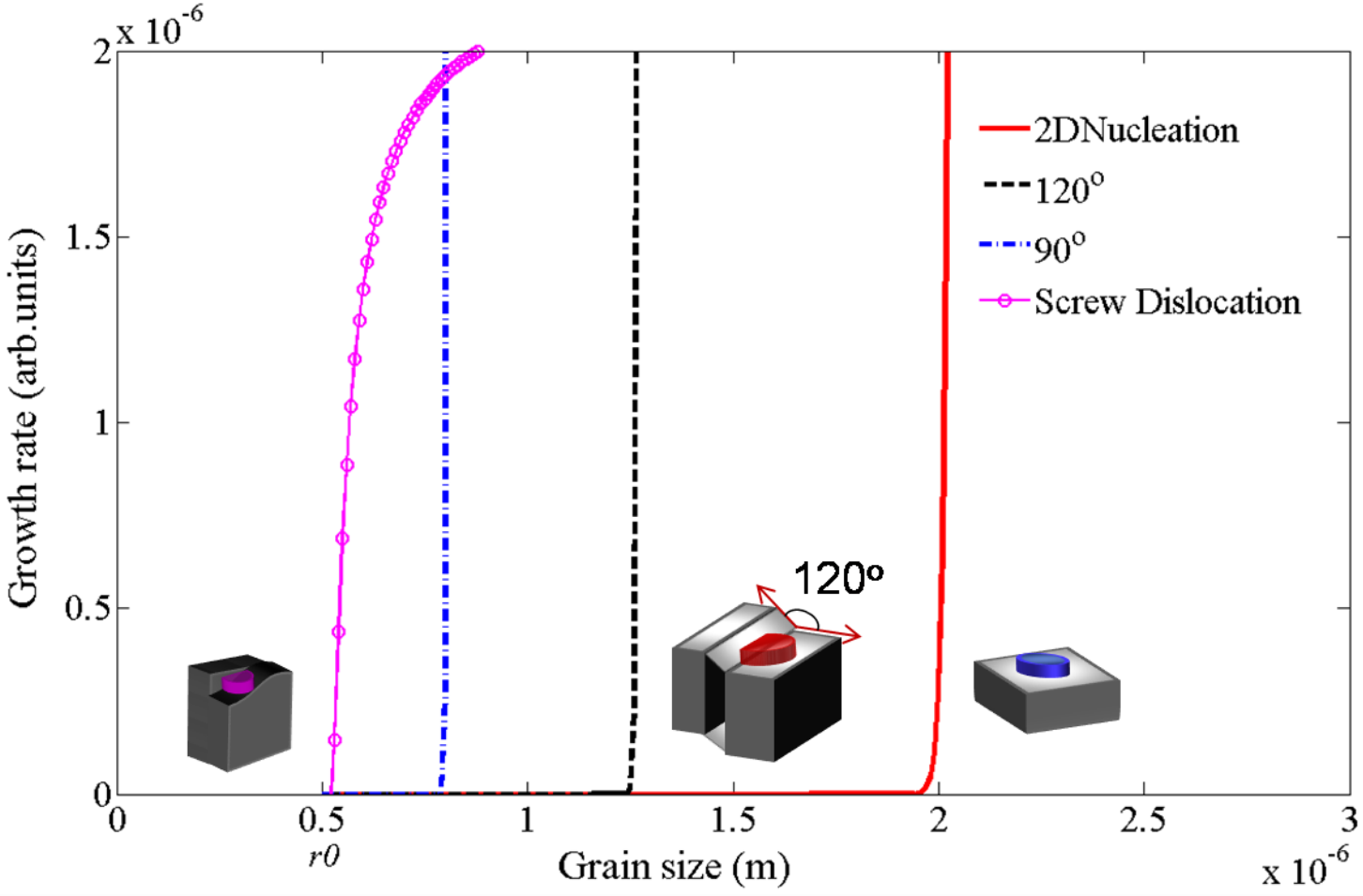

x 10^-6
2
1.5
1
0.5
0
Growth rate (arb.units)
2DNucleation
120°
90°
Screw Dislocation
120°
0
0.5
1
1.5
2
2.5
3
r0
Grain size (m)
x 10^-6

Fig. 10

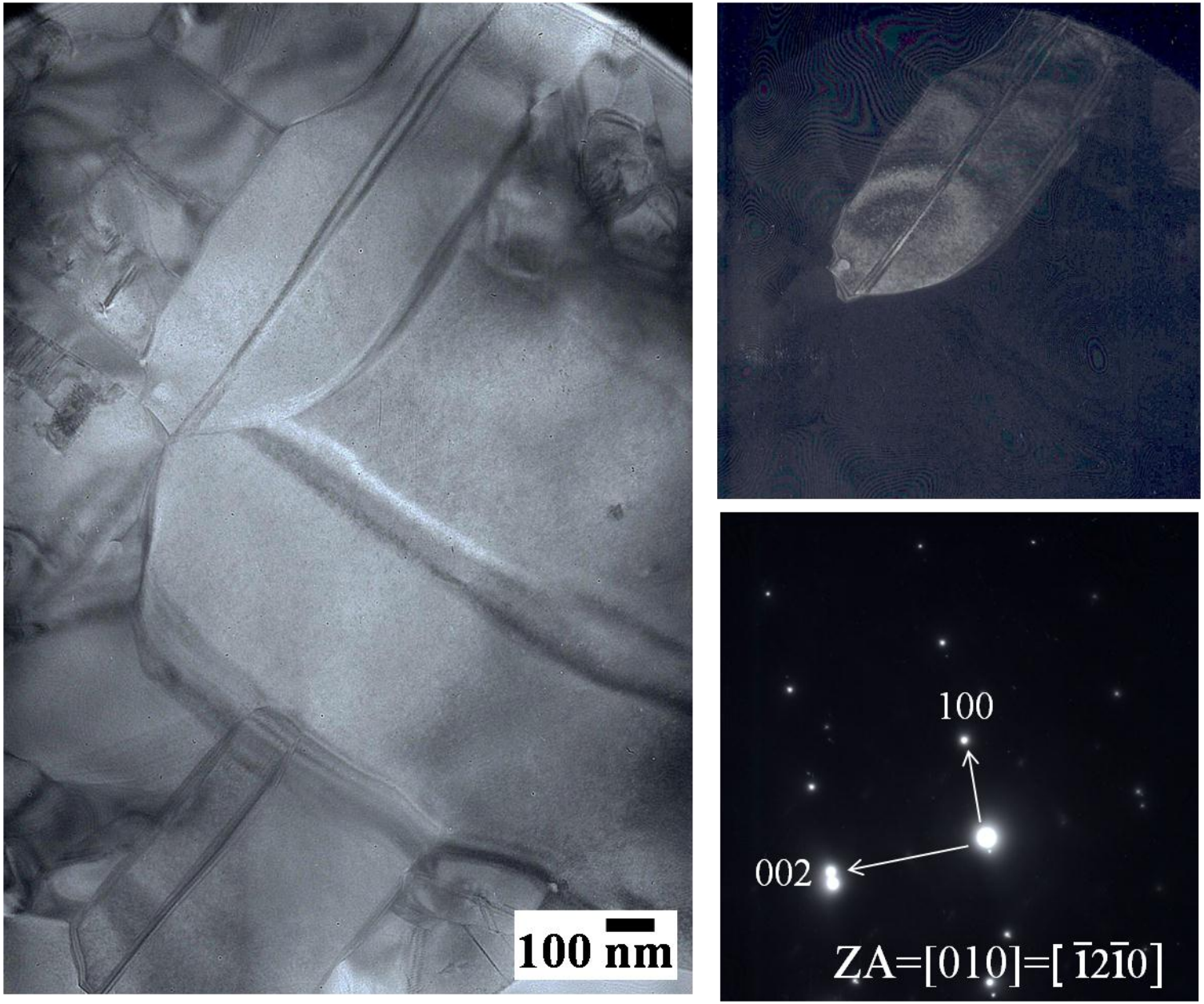


Fig. 11

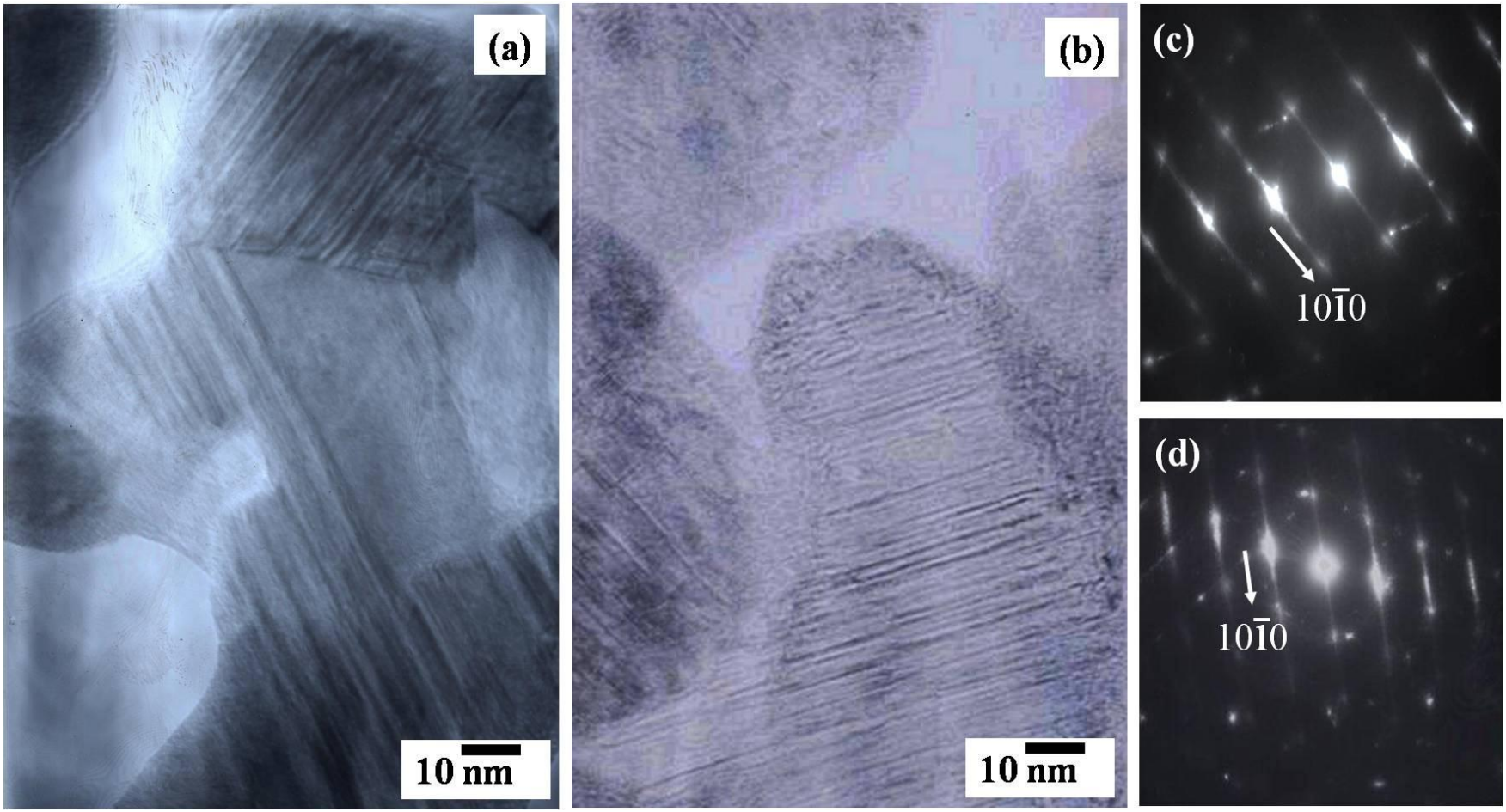


Fig. 12

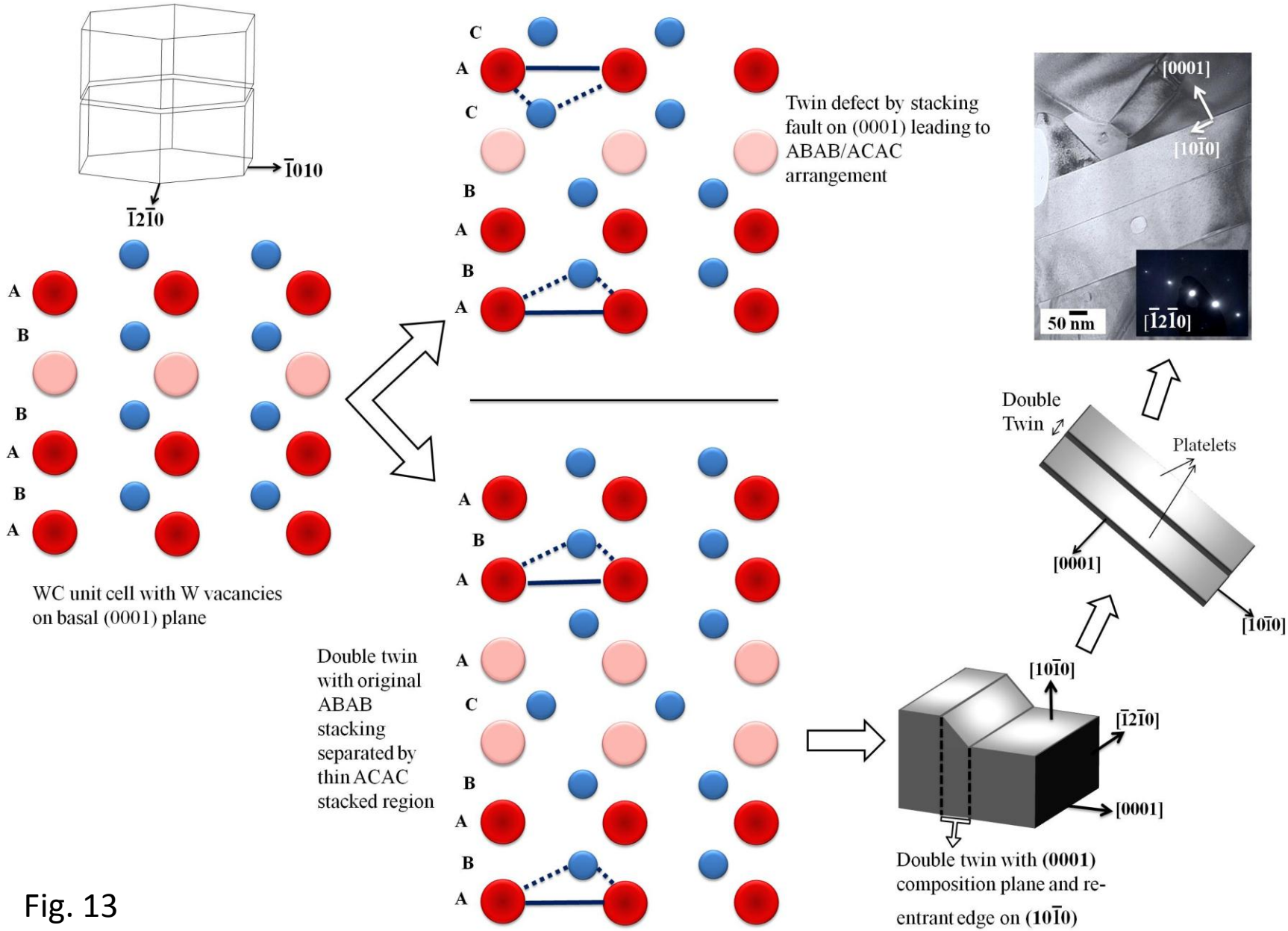
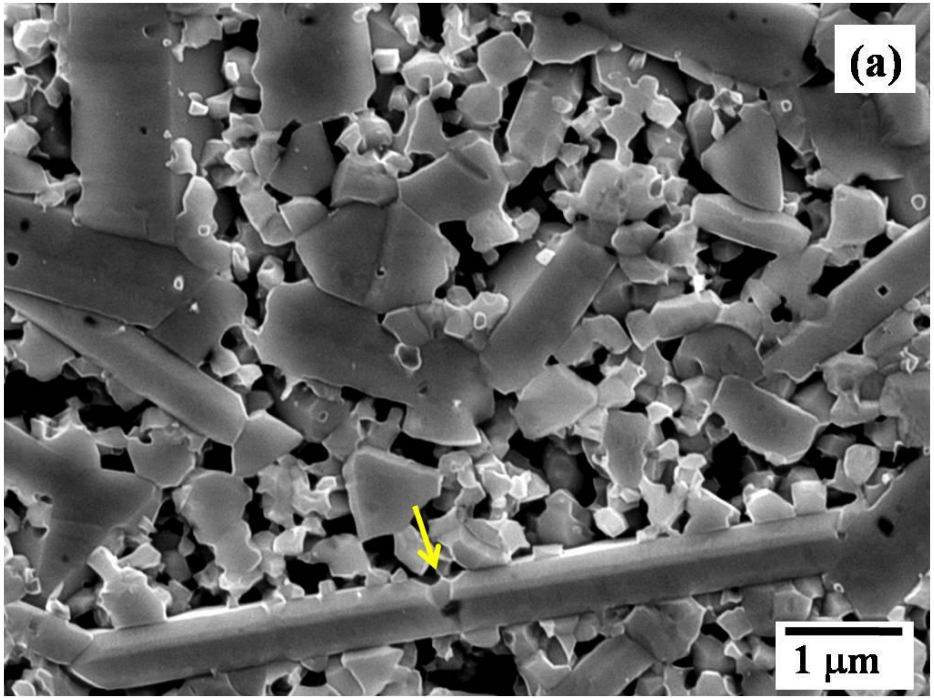

$\bar{1}010$
$\bar{1}2\bar{1}0$
A
B
B
A
B
A
C
A
C
B
A
B
A
Twin defect by stacking fault on (0001) leading to ABAB/ACAC arrangement
[0001]
$[10\bar{1}0]$
50 nm
$[\bar{1}2\bar{1}0]$
WC unit cell with W vacancies on basal (0001) plane
Double twin with original ABAB stacking separated by thin ACAC stacked region
A
B
A
C
B
A
B
A
Double Twin
Platelets
[0001]
$[10\bar{1}0]$
$[10\bar{1}0]$
$[\bar{1}2\bar{1}0]$
[0001]
Double twin with (0001) composition plane and re-entrant edge on $(10\bar{1}0)$

Fig. 13



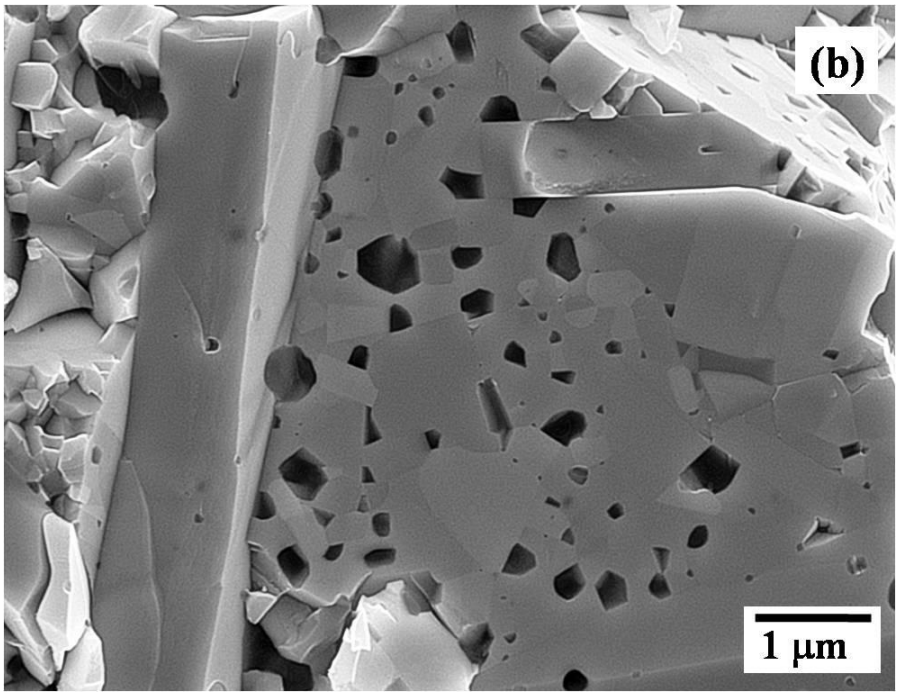


Fig. 14

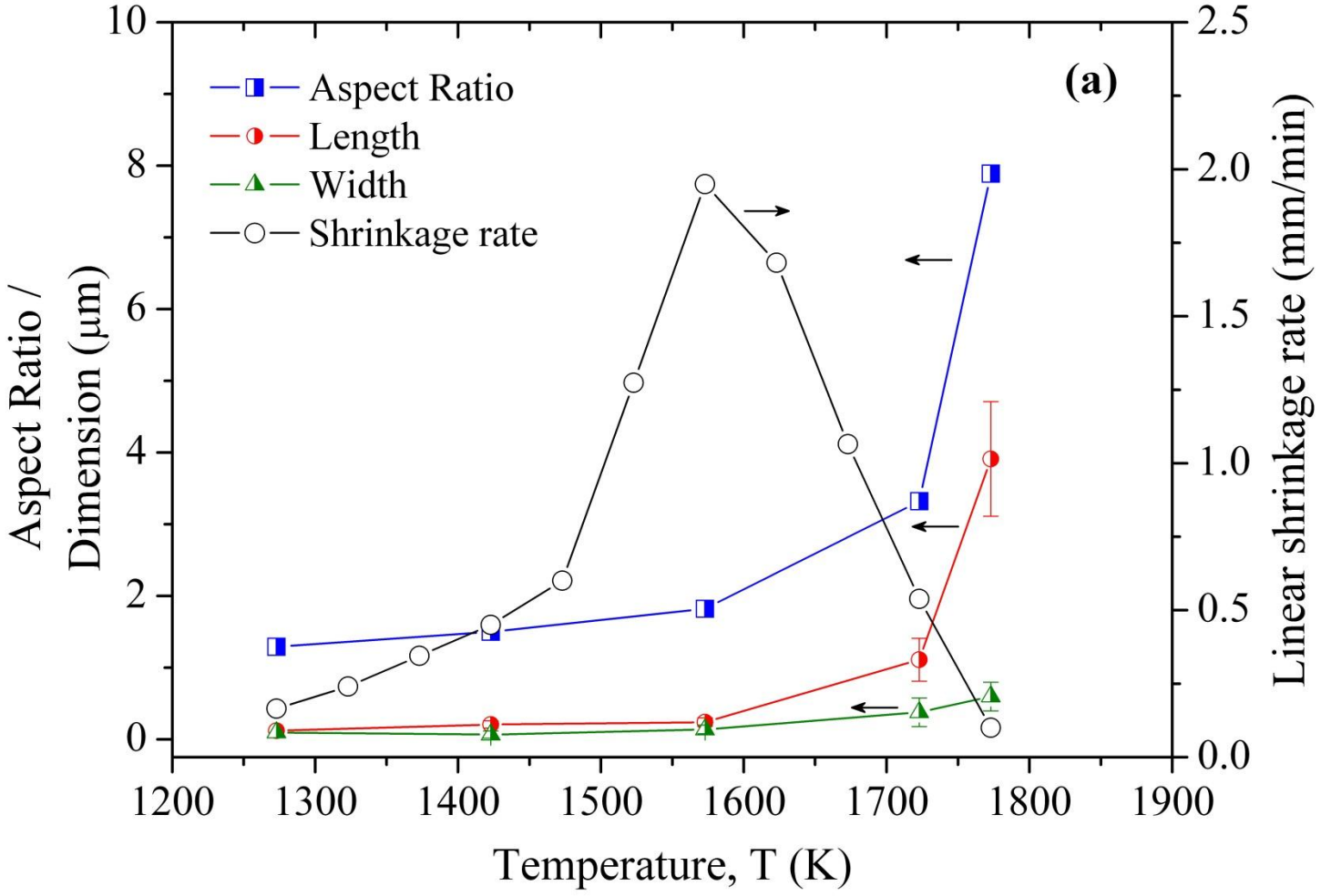

(a)
Aspect Ratio
Length
Width
Shrinkage rate
Aspect Ratio / Dimension (μm)
Linear shrinkage rate (mm/min)
Temperature, T (K)
10
8
6
4
2
0
2.5
2.0
1.5
1.0
0.5
0.0
1200
1300
1400
1500
1600
1700
1800
1900

Fig. 15

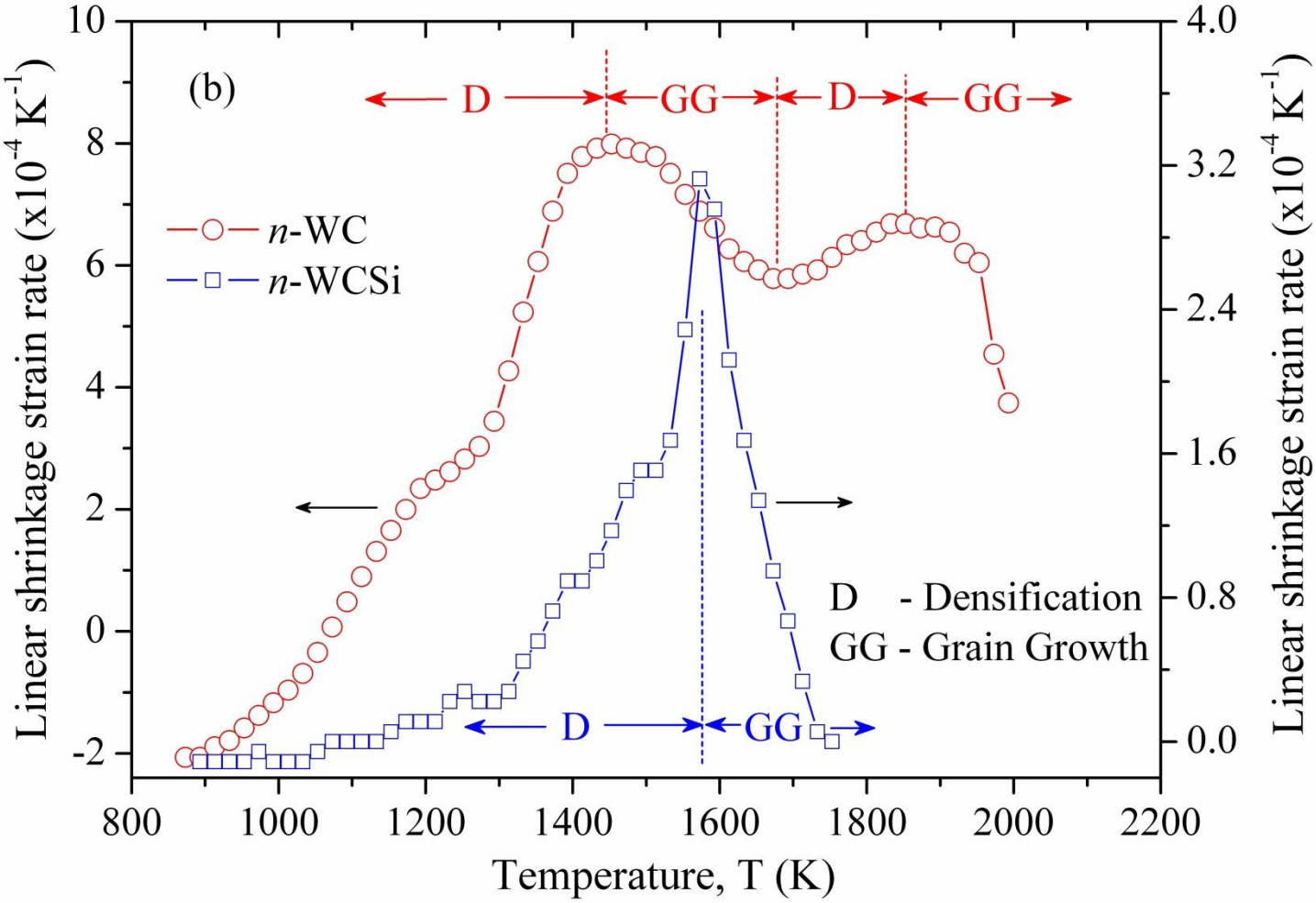

(b)
D
GG
D
GG
n-WC
n-WCSi
D - Densification
GG - Grain Growth
D
GG
Linear shrinkage strain rate (x10^{-4} K^{-1})
Linear shrinkage strain rate (x10^{-4} K^{-1})
Temperature, T (K)
10
8
6
4
2
0
-2
4.0
3.2
2.4
1.6
0.8
0.0
800
1000
1200
1400
1600
1800
2000
2200

Fig. 15